CLNS 94/1268
CLEO 94–3
January 27, 1994

Luminosity Measurement with the CLEO II Detector

G. Crawford,[1] C. M. Daubenmier,[1] R. Fulton,[1] D. Fujino,[1] K.K. Gan,[1] K. Honscheid,[1] H. Kagan,[1] R. Kass,[1] J. Lee,[1] R. Malchow,[1] Y. Skovpen,[1*] M. Sung,[1] C. White,[1] F. Butler,[2] X. Fu,[2] G. Kalbfleisch,[2] W.R. Ross,[2] P. Skubic,[2] M. Wood,[2] J. Fast,[3] R.L. McIlwain,[3] T. Miao,[3] D.H. Miller,[3] M. Modesitt,[3] D. Payne,[3] E.I. Shibata,[3] I.P.J. Shipsey,[3] P.N. Wang,[3] M. Battle,[4] J. Ernst,[4] L. Gibbons,[4] Y. Kwon,[4] S. Roberts,[4] E.H. Thorndike,[4] C.H. Wang,[4] J. Dominick,[5] M. Lambrecht,[5] S. Sanghera,[5] V. Shelkov,[5] T. Skwarnicki,[5] R. Stroynowski,[5] I. Volobouev,[5] G. Wei,[5] P. Zadorozhny,[5] M. Artuso,[6] M. Goldberg,[6] D. He,[6] N. Horwitz,[6] R. Kennett,[6] R. Mountain,[6] G.C. Moneti,[6] F. Muheim,[6] Y. Mukhin,[6] S. Playfer,[6] Y. Rozen,[6] S. Stone,[6] M. Thulasidas,[6] G. Vasseur,[6] X. Xing,[6] G. Zhu,[6] J. Bartelt,[7] S.E. Csorna,[7] Z. Egyed,[7] V. Jain,[7] K. Kinoshita,[8] K.W. Edwards,[9] M. Ogg,[9] A. Bellerive,[10] D.I. Britton,[10] E.R.F. Hyatt,[10] D.B. MacFarlane,[10] P.M. Patel,[10] B. Barish,[11] M. Chadha,[11] S. Chan,[11] D.F. Cowen,[11] G. Eigen,[11] J.S. Miller,[11] C. O'Grady,[11] J. Urheim,[11] A.J. Weinstein,[11] D. Acosta,[12] M. Athanas,[12] G. Masek,[12] H.P. Paar,[12] M. Sivertz,[12] J. Gronberg,[13] R. Kutschke,[13] S. Menary,[13] R.J. Morrison,[13] S. Nakanishi,[13] H.N. Nelson,[13] T.K. Nelson,[13] C. Qiao,[13] J.D. Richman,[13] A. Ryd,[13] H. Tajima,[13] D. Sperka,[13] M.S. Witherell,[13] M. Procario,[14] R. Balest,[15] K. Cho,[15] M. Daoudi,[15] W.T. Ford,[15] D.R. Johnson,[15] K. Lingel,[15] M. Lohner,[15] P. Rankin,[15] J.G. Smith,[15] J.P. Alexander,[16] C. Bebek,[16] K. Berkelman,[16] K. Bloom,[16] T.E. Browder,[16#] D.G. Cassel,[16] H.A. Cho,[16] D.M. Coffman,[16] P.S. Drell,[16] R. Ehrlich,[16] P. Gaiderev,[16] R.S. Galik,[16] M. Garcia-Sciveres,[16] B. Geiser,[16] B. Gittelman,[16] S.W. Gray,[16] D.L. Hartill,[16] B.K. Heltsley,[16] C.D. Jones,[16] S.L. Jones,[16] J. Kandaswamy,[16] N. Katayama,[16] P.C. Kim,[16] D.L. Kreinick,[16] G.S. Ludwig,[16] J. Masui,[16] J. Mevissen,[16] N.B. Mistry,[16] C.R. Ng,[16] E. Nordberg,[16] J.R. Patterson,[16] D. Peterson,[16] D. Riley,[16] S. Salman,[16] M. Sapper,[16] F. Würthwein,[16] P. Avery,[17] A. Freyberger,[17] J. Rodriguez,[17] R. Stephens,[17] S. Yang,[17] J. Yelton,[17] D. Cinabro,[18] S. Henderson,[18] T. Liu,[18] M. Saulnier,[18] R. Wilson,[18] H. Yamamoto,[18] T. Bergfeld,[19] B.I. Eisenstein,[19] G. Gollin,[19] B. Ong,[19] M. Palmer,[19] M. Selen,[19] J.J. Thaler,[19] A.J. Sadoff,[20] R. Ammar,[21] S. Ball,[21] P. Baringer,[21] A. Bean,[21] D. Besson,[21] D. Coppage,[21] N. Copty,[21] R. Davis,[21] N. Hancock,[21] M. Kelly,[21] S. Kotov,[21] I. Kravchenko,[21] N. Kwak,[21] H. Lam,[21] Y. Kubota,[22] M. Lattery,[22] M. Momayezi,[22] J.K. Nelson,[22] S. Patton,[22] D. Perticone,[22] R. Poling,[22] V. Savinov,[22] S. Schrenk,[22] R. Wang,[22] M.S. Alam,[23] I.J. Kim,[23] B. Nemati,[23] J.J. O'Neill,[23] H. Severini,[23] C.R. Sun,[23] and M.M. Zoeller[23]

(CLEO Collaboration)

∗ Permanent address: INP, Novosibirsk, Russia
Permanent address: University of Hawaii at Manoa

[1]Ohio State University, Columbus, Ohio, 43210
[2]University of Oklahoma, Norman, Oklahoma 73019
[3]Purdue University, West Lafayette, Indiana 47907
[4]University of Rochester, Rochester, New York 14627
[5]Southern Methodist University, Dallas, Texas 75275
[6]Syracuse University, Syracuse, New York 13244
[7]Vanderbilt University, Nashville, Tennessee 37235
[8]Virginia Polytechnic Institute and State University, Blacksburg, Virginia, 24061
[9]Carleton University, Ottawa, Ontario K1S 5B6 and the Institute of Particle Physics, Canada
[10]McGill University, Montréal, Québec H3A 2T8 and the Institute of Particle Physics, Canada
[11]California Institute of Technology, Pasadena, California 91125
[12]University of California, San Diego, La Jolla, California 92093
[13]University of California, Santa Barbara, California 93106
[14]Carnegie-Mellon University, Pittsburgh, Pennsylvania 15213
[15]University of Colorado, Boulder, Colorado 80309-0390
[16]Cornell University, Ithaca, New York 14853
[17]University of Florida, Gainesville, Florida 32611
[18]Harvard University, Cambridge, Massachusetts 02138
[19]University of Illinois, Champaign-Urbana, Illinois, 61801
[20]Ithaca College, Ithaca, New York 14850
[21]University of Kansas, Lawrence, Kansas 66045
[22]University of Minnesota, Minneapolis, Minnesota 55455
[23]State University of New York at Albany, Albany, New York 12222

(January 27, 1994)

Abstract

A measurement of absolute integrated luminosity is presented using the CLEO II detector operating at the CESR e^+e^- storage ring. Independent analyses of three different final states (e^+e^-, $\gamma\gamma$, and $\mu^+\mu^-$) at $\sqrt{s} \simeq 10$ GeV normalize to the expected theoretical cross sections and correct for detection efficiencies. The resulting luminosities are measured with systematic errors of $\pm 1.8\%$, $\pm 1.6\%$, and $\pm 2.2\%$, respectively, and are consistent with one another. The combined luminosity has a systematic error of $\pm 1.0\%$.

Submitted to *Nuclear Instruments and Methods*

1. Introduction

In this article we describe the determination of integrated luminosity in the CLEO II detector at the Cornell Electron Storage Ring (CESR), an e^+e^- collider operating at a center-of-mass energy of $\sqrt{s} \approx 10$ GeV. Knowledge of the luminosity is essential for many purposes. Analysis of Υ decays, including B meson physics in Υ(4S)$\rightarrow B\bar{B}$, commonly requires the *relative* luminosity in data taken on and off the resonance so that backgrounds from continuum production may be accurately subtracted. Frequently an analysis will make an internal consistency check by dividing the dataset into independent subsets of comparable size, again relying on accuracy and stability of the relative accumulated luminosity. The *absolute* luminosity is important for hadronic cross section determinations[1] both on and near the $\Upsilon(nS)$ resonances. Most demanding of precision in absolute luminosity are branching fraction measurements[2] of the tau lepton which normalize particular decay topologies to the total number of tau pairs produced.

To minimize both theoretical and systematic uncertainties, the approach taken here is to separately analyze three different processes which have large and well-known cross sections: final state pairs of electrons, photons, and muons. Experimentally, the response of the detector to each of these reactions is quite distinct: the efficiencies rely on charged particle tracking, calorimetry, and triggering in different ways for each process. The expected theoretical cross sections are calculable in quantum electrodynamics; weak interaction effects are negligible. The primary theoretical obstacle in all cases is computation of the electromagnetic radiative corrections in a way that accomodates experimental event selection criteria and achieves adequate precision. This is most conveniently accomplished with a Monte Carlo event generator which properly includes diagrams with a varying number of virtual and real radiative photons to consistent order in α.

The general procedure for computing luminosity is the same for all three analyses. Event selection criteria cleanly isolate the desired events, which are tallied for each CLEO "run", usually half of a one-hour CESR fill. Second, one or more event generators are used in conjunction with a detailed detector simulation to compute a cross section corrected for event selection criteria and dominant radiative effects. To obtain luminosity, event tallies are decremented for estimated backgrounds, and then divided by the expected cross sections corrected for trigger and selection efficiencies. For a dataset of $\sim$2.5 fb^{-1}, the stability of relative luminosities from the three processes are compared. Finally, the three measurements are combined into a single absolute luminosity.

2. The CLEO II Detector

CLEO II is a general purpose detector[3] investigating heavy quark decays, tau physics, Υ spectroscopy, quark fragmentation, and two-photon interactions. The components most important for the luminosity analyses are the trigger system, tracking chambers, and the calorimeter. A set of three concentric drift chambers in a 1.5 T axial magnetic field provides charged particle momentum measurements with resolution σ_p/p (%) $\simeq \sqrt{(0.15p)^2 + (0.5)^2}$, p in GeV/c. These chambers have 67 cylindrical layers of drift cells centered on the beam line, with radii from 4.7-90 cm. Track $z-$coordinates[4] are measured with eleven stereo layers and four planes of cathode strips. The beam pipe, chamber walls, gas, and wires together constitute 0.028 radiation lengths of material at normal incidence between the nominal interaction point (IP) and last drift chamber layer. Surrounding the drift chambers but inside the superconducting magnet coil, an array of 7800 CsI(Tl) crystals with silicon photodiode readout is divided into a barrel region and two endcaps. The 6144 barrel crystals, arranged in a projective geometry, surround the tracking chambers at $\sim$1 m radius, covering $|\cos\theta| < 0.82$. Two identical endcaps, each containing 828 rectangular crystals, occupy $0.80 < |\cos\theta| < 0.98$, and complete the hermetic coverage over 98% of the solid angle. The barrel calorimeter achieves energy and angular resolutions, respectively, of σ_E/E (%) $= 0.35/E^{0.75} + 1.9 - 0.1E$ and σ_ϕ (mrad)$=2.8/\sqrt{E} + 2.5$, E in GeV. Muons are detected by their penetration through one or more of three slabs of magnet iron 36 cm thick located outside the coil, where three layers of Iarocci tube chambers instrument the gap behind each slab.

Fast trigger signals and particle time-of-flight (TF) are provided by 5 cm-thick scintillation counters located just inside the calorimeter in the barrel and endcap. The 64 barrel TF counters are 279 cm long by 10 cm wide, are aligned parallel to the beams, and are read out by photomultiplier tubes at both ends. A three-tier hardware trigger system[5] takes input from the calorimeter, tracking chambers, and TF counters to form different combinations of requirements, or "lines", that force readout of the entire detector. At the lowest level trigger, L0, simple and fast criteria reduce the 2.7 MHz beam-crossing frequency to a manageable rate. The more complex logical conditions which are input at the next level, L1, are ready for interrogation about 1 μs after an L0. The readiness time for the third level, L2, is $\sim$50 μs. At CESR luminosities typical of the past two years (2×10^{32}cm^{-2}sec^{-1}), the L0/L1/L2 trigger rates are $\sim$11k/35/25 Hz, resulting in a dead-time of $\sim$8%. A fourth-level trigger (L3) implemented in software processes information assembled from the entire detector to reject about half the L2 triggers as uninteresting cosmic rays or interactions of the beam particles with gas or vacuum chamber walls. Every 200-th event failing L2 and every eighth failing L3 criteria are flagged but retained in the data stream for subsequent monitoring of trigger performance.

3. Event Selection

Luminosity events are triggered, acquired, and analyzed in the same manner as all physics events. Hence event tallies are guaranteed to be immune from additional corrections due to dead-time, offline analysis procedures, or errors in data handling. In a typical CLEO run of 250 nb^{-1}, the selection criteria below would count $\sim$2100 Bhabha events, $\sim$280 photon pair events, and $\sim$90 muon pair events. There is another less precise but higher rate monitor of luminosity. Coincidences of back-to-back beam energy showers detected in the endcap CsI calorimeters with online hardware provide a luminosity estimate during data acquisition. This monitor counts at a rate of $\sim$28 Hz at 2×10^{32}cm^{-2}sec^{-1}, and is used for tuning CESR beam conditions and for online CLEO diagnostics. It plays no role in the luminosity computation presented here, although it is routinely cross-calibrated with this analysis.

Each of the reactions has its own unique signature in the detector which motivates event selection criteria. Bhabha events have two high-momentum charged tracks and two high energy showers in the calorimeter, whereas photon pairs, which also shower, usually leave no tracks. The two primary showers in $\gamma\gamma$ events tend to be back-to-back in azimuth. However, the showers in Bhabha events are slightly away from back-to-back because the e^+ and e^- travel helical trajectories in the magnetic field. In contrast, while muon pair events also have two stiff tracks, each leaves only a minimum-ionizing ($\sim$220 MeV) shower in the calorimeter. Large calorimeter energy deposition gives Bhabhas and $\gamma\gamma$'s a near-perfect trigger efficiency. Muon pair events elude the CLEO II trigger $\sim$15% of the time by failing calorimeter energy or tracking requirements, or by passing through gaps between TF counters.

Bhabhas and photon pairs are the most likely background for each other because of their similarity in calorimetric energy deposition and relatively large cross sections. Selection criteria for Bhabha events must also discriminate against cosmic rays, tau pair events where both tau's decay

Table 1: Luminosity Event Selection Criteria

#	Description	e^+e^-	$\gamma\gamma$	$\mu^+\mu^-$
1	# CsI showers	$\geq$2	$\geq$2	$\geq$2
2	Shower Energy	$(0.5-1.1)E_b$	$> 0.5E_b$	$(0.15-0.5)$ GeV
3	Shower acoplanarity	>0.05	<0.03	–
4	# charged tracks	$\geq$2	≤ 1	=2
5	$\lvert\cos\theta_1\rvert$	<0.707	<0.707	<0.707
6	$\lvert\cos\theta_2\rvert$	<0.766	<0.766	<0.766
7	Track acollinearity	<40°	–	<8°
8	Track momentum	$> 0.5P_b$	–	$(0.75-1.15)P_b$
9	Track impact parameter	–	–	< 1.5 mm
10	Track z nearest IP	–	–	< 60 mm
11	$\cos\theta_1 \times \cos\theta_2$	<0.001	<0.001	<0
12	Trigger line	ENERGY	ENERGY	MUPAIR

electronically, and $e^+e^-e^+e^-$ final states. Cosmic rays are the primary source of fake muon pairs, although tau pairs and the two-photon process $e^+e^-\mu^+\mu^-$ can potentially contribute as well.

The event selection criteria are summarized in Table 1. There must be at least two calorimeter showers in every event, and, for Bhabhas and $\gamma\gamma$'s, they must exceed half the beam energy E_b.[6] The acoplanarity of the showers, defined as their azimuthal acollinearity in radians, must be less than 0.03 in $\gamma\gamma$ events, and must exceed 0.05 in Bhabha events, to further exclude each class from contaminating the other. Two good [7] tracks must be found in Bhabhas and $\mu-$pairs, and zero or one are permitted in $\gamma\gamma$'s.[8] Both tracks in $\mu-$pair events must "match" showers (project to within 8 cm of a member crystal) summing to (0.15-0.5) GeV, typical of minimum-ionizing particles. The tracks in Bhabha and muon pair events must have acollinearity less than 40° and 8°, respectively. For the Bhabhas, this acollinearity requirement restricts the event topology to a region simulated well by the event generators. The somewhat more restrictive requirement for $\mu^+\mu^-$ events ensures that the trigger efficiency can be calculated accurately. Both good tracks in Bhabha events have momenta exceeding half the beam momentum P_b. Both tracks in $\mu-$pair events must have momenta in the range $(0.75-1.15)P_b$. Events are restricted to the angular region with the best trigger and detector response by requiring both tracks, or for $\gamma\gamma$'s, both showers, to have $|\cos\theta| < 0.766$, and at least one with $|\cos\theta| < 0.707$. This asymmetry in the angular cutoffs reduces dependence on detector angular resolution and position of the interaction point. Cosmic rays remaining in the $\mu^+\mu^-$ sample are reduced further by requiring both tracks to have impact parameters[7] $|d_\pm|$ <1.5 mm and z-coordinate nearest the IP $|z_0|$ <60 mm. For reliable triggering in all three event classes, the two largest showers must lie in opposite halves of the calorimeter, as split by a plane at $z=0$. All Bhabha and $\gamma\gamma$ events must trigger on the ENERGY line, and muon pairs on the MUPAIR line, both of which will be described in the following section.

4. Trigger Efficiency

Bhabha and $\gamma\gamma$ events, as selected, trigger the detector on the ENERGY line. ENERGY requires at least two 4×4-crystal groupings to exceed the CBHI (Crystal Barrel HIgh) threshold of ~0.5 GeV. The two groupings must be located in opposite halves of the calorimeter (as divided by the plane $z = 0$). Since each of the top two showers is already required to deposit more than half the beam energy, 2CBHI is satisfied for most events, even in the limiting case of a shower dividing its energy equally among four 16-crystal trigger groupings. The efficiency can be measured with the data because there is another trigger line (ELTRACK) which requires only 1CBHI (and $\geq$1 track in the drift chambers). For Bhabha events, the fraction of ELTRACK triggers also satisfying the ENERGY line, which yields the 1CBHI efficiency, is (99.85$\pm$0.01)%. This must be squared to obtain the 2CBHI efficiency of (99.70$\pm$0.02)%. This value can be applied to $\gamma\gamma$'s as well due to the similarity of energy deposition. A Monte Carlo simulation of the detector trigger predicts (99.65$\pm$0.02)% ENERGY efficiency for Bhabhas and (99.59$\pm$0.03)% for $\gamma\gamma$'s, supporting the assigned efficiencies.

There is a correction to the trigger efficiency for Bhabha events. At least one barrel TF counter must fire at L0 (1TF) in order for charged tracks to be reconstructed because the L0 ENERGY signal comes too late to correctly latch the drift chamber hits. However, not every Bhabha event satisfies 1TF because the TF trigger efficiency falls off near the azimuthal counter edges. The rate for such triggers has been estimated directly from the data by visually scanning events which satisfy all Bhabha criteria except the track requirement. Many such events can be seen to have a few residual hits along the $e^{\pm}$ direction, though others are clearly $\gamma\gamma$'s or cosmic rays. The fraction of Bhabha events with exclusive L0 ENERGY triggers without 1TF is (0.8$\pm$0.4)%, where the error accounts for statistics and ambiguities in identifying scanned events. This reduces the Bhabha event trigger efficiency to 98.9%.

The MUPAIR line efficiency for $\mu^+\mu^-$ events is much lower and more difficult to determine. The MUPAIR line requires two barrel TF counters (2TF), two calorimeter deposits exceeding the CBLO threshold of $\sim$0.1 GeV and located in opposite halves of the barrel, and two tracks found by the trigger system. The TF requirement was relaxed to 1TF for the last third of the dataset. CBLO can fail near the edges of 16-crystal trigger groupings when not enough energy is deposited in either grouping. Care must be taken to account properly for correlations: $\mu-$pairs tend to be back-to-back, and gaps between TF counters align closely in azimuth with crystal-grouping edges. Hence when one muon fails CBLO or TF, both muons are likely to fail. In addition, the L3 software filter tends to reject some true $\mu-$pairs because they are erroneously tagged as cosmic rays.

The total MUPAIR trigger efficiency for events passing the $\mu^+\mu^-$ selection criteria is (85.3$\pm$1.1)%. It is the product of four independent efficiencies, all of which are calculated from the data: tracking, 2TF and 2CBLO near the center of counters, 2TF*2CBLO near TF counter edges, and L3 losses. The tracking trigger efficiency, calculated using Bhabha events which trigger on the ENERGY line and corrected the lower ionization of muons, is (97$\pm$1)%. The L3 efficiency of (98.0$\pm$0.5)% is obtained from the fraction of all events flagged as L3 rejects.

The 2TF and 2CBLO efficiencies in the central half of a TF counter are calculated from a set of events satisfying a different trigger line, one which requires only 1TF and 1CBLO. (This line also has more restrictive tracking requirements than MUPAIR, so it only fires on 7% of all selected $\mu-$pairs.) When the μ^+ is incident within 2.5 cm of the center of a 10 cm-wide TF counter in azimuth, but anywhere along its length, the 2TF efficiency for the event is found to be (99.5$\pm$0.1)%, and the 2CBLO efficiency is (96.6$\pm$0.5)%, where the errors include statistics and systematic uncertainties in the technique. Because of correlations, in the 2.5 cm near each azimuthal TF edge, only the combined 2TF*2CBLO efficiency is calculated. It is obtained by examining the distribution of ϕ_{TF}, the projected μ^+ azimuthal intercept, modulo a half-TF counter width, as shown in Fig. 1, where ϕ_{TF}=0 corresponds to an edge and ϕ_{TF}=1 is the counter center. The combined 2TF*2CBLO efficiency, taken as the number of entries in the plot divided by twice the number with $\phi_{TF}>0.5$, is $(92.4\pm0.5)\%$. For the last third of the dataset in which only 1TF is required, the 1TF efficiency in the center of a counter is $(99.9\pm0.1)\%$, and the combined 1TF*2CBLO efficiency near the counter edges is $(97.4\pm0.5)\%$.

In summary, the trigger efficencies for e^+e^-, $\gamma\gamma$, and $\mu^+\mu^-$ are $(98.9\pm0.5)\%$, $(99.7\pm0.1)\%$, and $(85.3\pm1.1)\%$, respectively, where the errors include estimates of all systematic and statistical uncertainties. For the $\mu-$pairs, this value represents the average of the efficiencies computed for eight consecutive run ranges of comparable luminosity; due to changing trigger conditions, the components of the $\mu-$pair trigger efficiency must be recomputed for each range.

5. Acceptance

The acceptance, or efficiency-corrected cross section, is computed for each reaction using at least one event generator coupled with a detailed, GEANT-based detector simulation.[9] In each case radiative photons are generated above some photon energy cutoff $k_0 = E_\gamma/E_b$, and all diagrams with softer photons are subsumed into the two-body final state. Two generators each were used for e^+e^- and $\mu^+\mu^-$ scattering, and one for $\gamma\gamma$ events. The BKee program[10] generates e^+e^- final states with zero or one radiative photon, yielding a cross section accurate to order-α^3. Higher order corrections are available in the BHLUMI program[11], which uses Yennie-Frautschi-Suura exponentiation to generate many photons per event and yields a cross section accurate to order $\sim \alpha^4\ln^2(|t|/m_e^2)$, where t is the typical momentum-transfer. As with BKee, the BK$\gamma\gamma$ Monte Carlo[12] generates $\gamma\gamma$ events with up to one radiative photon and yields an order-α^3 cross section, as does the BKJ generator[13] for $\mu-$pairs. Up to three radiative photons in $\mu^+\mu^-$ events are possible (two from initial state radiation and one from final state radiation) with FPAIR[14], which has an order-α^4 accuracy. A photon cutoff of k_0=0.01 is used for BKee, BK$\gamma\gamma$, and BKJ, and k_0=0.001 for BHLUMI and FPAIR. Acceptances are quoted at E_b=5.29 GeV, with corrections for the actual beam energy made on a run-by-run basis. Acceptance does not include trigger efficiency.

Table 2: Acceptance at E_b=5.29 GeV

Item	e^+e^-	$\gamma\gamma$	$\mu^+\mu^-$
α^2 Acceptance (nb)	8.48 ± 0.02	1.176 ± 0.002	0.467 ± 0.001
α^3 Generator	BKee	BK$\gamma\gamma$	BKJ
α^3 Acceptance (nb)	8.45 ± 0.02	1.124 ± 0.002	0.429 ± 0.001
α^4 Generator	BHLUMI	–	FPAIR
α^4 Acceptance (nb)	8.34 ± 0.02	–	0.427 ± 0.001

The acceptances for different orders of radiative corrections are given in Table 2. Relative first order corrections are -0.4%, -4.6%, and -8.1%, respectively, for Bhabhas, $\gamma\gamma$'s, and $\mu-$pairs, whereas the second order corrections are -1.3%, unknown, and -0.5%. For Bhabhas and $\mu-$pairs the α^4 acceptances are used for luminosity; for photon pairs, where no α^4 generator is available, the α^3 acceptance is used.

Distributions of variables significant for acceptance are shown in Figs. 2, 3, and 4. Agreement between data[15] and Monte Carlo is generally quite good, but there are discrepancies which indicate imperfect event generation and/or detector simulation. In particular, data distributions are slightly broader than Monte Carlo in acoplanarity and shower energy for $\gamma\gamma$'s and track momentum for

$\mu-$pairs (Figs. 3(a), 3(c), and 4(c), respectively). However, the acceptances are not seriously biased by such differences because the cuts are placed where event populations are very low, far from the regions of disagreement. Similarly, Fig. 4(d) shows that the muon calorimeter energy spectrum in the detector Monte Carlo is too hard at low energy. But the $\mu^+\mu^-$ acceptance is unaffected, since the efficiency for exceeding 0.15 GeV and satisfying the CBLO trigger requirement is computed from the data directly, not the simulation. Differences between data and Monte Carlo are quantified by assigning systematic errors to the acceptance which accomodate changes induced by reasonable variations in all the selection criteria. This procedure results in errors attributed to inadequate detector modeling of 1.1%, 0.9%, and 1.4% for the e^+e^-, $\gamma\gamma$, and $\mu^+\mu^-$ final states, respectively.

The higher-order event generators (BHLUMI for Bhabhas and FPAIR for $\mu-$pairs) are intended to yield more realistic event kinematics as well as more accurate overall normalization. There is an indication in the acollinearity and momentum distributions for $\mu-$pair events that this is true. The distributions of first, second, and third highest energy photons per event, shown in Fig. 5(a) for e^+e^- and Fig. 5(b) for $\mu^+\mu^-$, are even more sensitive to the order of radiative corrections. They verify that BHLUMI and FPAIR handle radiative photons in a more realistic manner than their order-α^3 counterparts (BKee and BKJ). The effect is less apparent for Bhabha events at low energies where many showers originate as bremsstrahlung in material or as satellites of the primary shower in the CsI crystals. These two sources of showers not attributable to photons from the primary vertex have nearly identical rates in both Bhabha Monte Carlos after detector simulation. The analogous distributions for the $\gamma\gamma$'s in Fig. 3(d) show only small discrepancies with the α^3 Monte Carlo (BK$\gamma\gamma$).

Systematic errors accounting for accuracy and adequacy of the theoretical radiative corrections in the Monte Carlo generators are taken as 1.3%, 1.3%, and 1.0% for the e^+e^-, $\gamma\gamma$, and $\mu^+\mu^-$ final states, respectively. These estimates are based on a number of considerations, including the technical precision and theoretical accuracy of the generators,[10– 14] agreement between data and Monte Carlo of important kinematical distributions (e.g. Figs. 2–5), consistency of the α^3 and α^4 predictions in Table 2, and stability of the results (<1%) with respect to reasonable variations in the photon energy cutoff k_0.

6. Backgrounds

Cosmic rays dominate the background in the $\mu-$pair sample. Tight track quality requirements minimize this contamination with almost no loss in efficiency. The remaining cosmic background is estimated with two independent variables, impact parameter and time-of-flight. For the first method, the distribution of μ^- impact parameter d_- is compared with that from a relatively pure sample of cosmic rays. To obtain the cosmic ray sample, a variable based on time-of-flight is required to be inconsistent with the event originating as an e^+e^- interaction: $T = \sqrt{{t_+}^2 + {t_-}^2} >$4 ns, where t_+ (t_-) is the time recorded by the TF counter struck by the μ^+ (μ^-) relative to the expected time. Fig. 6(a) shows d_- on events for which the impact parameter requirement has been loosened from 1.5 mm to 3.0 mm, overlaid with that of the cosmic sample, which has been normalized in the tail region $|d_-| > 2$ mm. The small enhancement near zero in the cosmic ray curve is due to the presence of true $\mu-$pairs in this subsample from TF mismeasurement. Accounting for this effect, the fraction of cosmic rays with $|d_-| < 1.5$ mm is (0.5±0.1)%. For the time-of-flight method, the fraction $\mu-$pairs that have $T >$4 ns (see Fig. 6(b)) is (0.6±0.1)%, in good agreement with the impact parameter method. Background from tau-pair decays, according to the KORALB[16] Monte Carlo, is 0.07%, and from $ee\mu\mu$ events[17] is <0.002%.

The background in photon pair events from Bhabhas that have no tracks (because they do not fire an L0 TF trigger) can be easily estimated. The product of the probability for a Bhabha to have no tracks (~0.8%), the probability for a Bhabha to satisfy all the $\gamma\gamma$ criteria *except* zero or one track (~1.5%), and the ratio of the Bhabha to $\gamma\gamma$ acceptance yields a relative background of (0.1±0.1)%. There is no evidence for any other significant backgrounds in the $\gamma\gamma$ sample.

For Bhabhas, tau pairs contribute 0.03% background. A Monte Carlo generator[18] for the final state $e^+e^-e^+e^-$ yields an estimate of (0.05±0.05)% background. The level of cosmic rays in the sample can be estimated in three ways, two of which are similar to the techniques used for $\mu-$pairs. The time-of-flight variable T and the tails of the track impact parameter distribution show no evidence of cosmic rays. Only 0.05% of all events have one reconstructed muon track penetrating the first layer of magnet iron, and only 0.0015% have two, indicating the level of cosmic rays must be small. The total background in e^+e^- events is assumed to be (0.1±0.1)%.

7. Results

When the given trigger efficiencies, acceptances, and backgrounds are applied to the relevant event tallies, the resulting luminosities from the three final states are consistent with each other within errors. Averaged over the entire ~2.5 fb^{-1} dataset,[19] the ratio of the $\gamma\gamma$ to Bhabha luminosity is

$$\mathcal{L}(\gamma\gamma)/\mathcal{L}(e^+e^-) = 0.990 \pm 0.001,$$

and the ratio of the $\mu-$pair to Bhabha luminosity is

$$\mathcal{L}(\mu^+\mu^-)/\mathcal{L}(e^+e^-) = 0.997 \pm 0.002,$$

where the errors are statistical. Fig. 7(a) shows the time dependence of the $\gamma\gamma$ to Bhabha luminosity ratio in bins of ~40 pb^{-1}, and Fig. 7(b) the $\mu-$pair to Bhabha ratio in bins of ~125 pb^{-1}, both with statistical errors only. Both ratios are quite stable. Using the statistical errors, the χ^2 for ratios to be constant are 57 for 56 d.o.f. and 75 for 18 d.o.f., respectively. Hence there are no time-dependent systematic effects for $\gamma\gamma$'s and Bhabhas, but the $\mu-$pair statistical errors need to be doubled to bring the χ^2/d.o.f. down to unity. The systematic error already assigned to the $\mu-$pair trigger efficiency accounts for the substantial changes in trigger conditions over time.

Table 3: Relative Errors (%) in Luminosity

Source	e^+e^-	$\gamma\gamma$	$\mu^+\mu^-$
Monte Carlo Statistics	0.2	0.2	0.2
Trigger Efficiency	0.5	0.2	1.3
Backgrounds	0.1	0.1	0.1
Detector Modeling	1.1	0.9	1.4
Radiative Corrections	1.3	1.3	1.0
Summed in Quadrature	1.8	1.6	2.2

Table 3 summarizes the sources of error in the luminosity measurements. When all sources are combined in quadrature, Bhabhas, $\gamma\gamma$'s, and $\mu-$pairs yield results with comparable systematic errors (1.8%, 1.6%, and 2.2%, respectively). The trigger efficiency, backgrounds, and acceptance are assumed to be independent of one another, and the errors uncorrelated, so that the measurements may be combined into a single result. The error-weighted average of the three results is $0.995\mathcal{L}(e^+e^-)$. This combined luminosity has a $\pm 1.0\%$ systematic uncertainty.

8. Conclusion

The luminosity plays a crucial role in many physics measurements at an e^+e^- collider. We have presented three independent determinations of this quantity in the CLEO II detector, using e^+e^-, $\gamma\gamma$, and $\mu^+\mu^-$ final states produced at wide angles to the beam. Combining the three results, which are consistent with each other and have comparable errors, yields a relative systematic error of $\pm 1.0\%$.

The BHLUMI (e^+e^-) and FPAIR ($\mu^+\mu^-$) order-α^4 event generators are found to yield efficiency-corrected cross sections consistent at the $\sim 1\%$ level with their order-α^3 analogs (BKee and BKJ, respectively). The measured energy spectra of multiple radiative photons per event in the Bhabhas and $\mu-$pairs are reproduced by the α^4 generators.

9. Acknowledgements

We gratefully acknowledge the effort of the CESR staff in providing us with excellent luminosity and running conditions. J.P.A. and P.S.D. thank the PYI program of the NSF, I.P.J.S. thanks the YI program of the NSF, G.E. thanks the Heisenberg Foundation, K.K.G., I.P.J.S., and T.S. thank the TNRLC, K.K.G., H.N.N., J.D.R., T.S., and H.Y. thank the OJI program of DOE and P.R. thanks the A.P. Sloan Foundation for support. This work was supported by the National Science Foundation and the U.S. Dept. of Energy.

REFERENCES

1. D.S. Akerib *et al.*, Phys. Rev. Lett. 67 (1991) 1692.
2. D.S. Akerib *et al.*, Phys. Rev. Lett. 69 (1992) 3610; D.S. Akerib *et al.*, Phys. Rev. Lett. 71 (1993) 3395.
3. CLEO Collab., Y. Kubota *et al.*, Nucl. Instrum. and Meth. A320 (1992) 66.
4. The CLEO coordinate system has x pointing radially outward from the center of the CESR ring, y upward, and z along the positron direction. The polar angle θ is measured with respect to the $z-$axis, and azimuth ϕ in the $x-y$ plane with respect to the $x-$axis.
5. C. Bebek, et al., Nucl. Instr. and Meth. A302 (1991) 261.
6. To exclude cosmic rays in Bhabha events, showers cannot exceed $1.1E_b$; there is no such upper bound for $\gamma\gamma$'s because cosmics tend not to be back-to-back in azimuth.
7. Bhabha events with an extra track or two from a $\delta-$ray or low-energy photon conversion are kept in the sample by defining a "good" track (for this class only) as having either momentum exceeding 0.15 GeV/c or smaller than 1 cm impact parameter (distance of closest approach to the beam-axis in the plane transverse to the beam).
8. Single track $\gamma\gamma$ events are additionally required to have the second highest shower energy exceed $0.9E_b$. True $\gamma\gamma$ events with an erroneously found track will tend to satisfy this requirement. Single track events which fail to satisfy it appear (from event scanning) to be highly radiative Bhabha events where one electron has been reconstructed and the other has disappeared at extreme polar angle.

9. R. Brun *et al.*, GEANT v. 3.14, CERN DD/EE/84-1. Version 3.15 is used here.
10. F. Berends and R. Kleiss, Nucl. Phys. B228 (1983) 537.
11. S. Jadach, E. Richter-Was, B.F.L. Ward, and Z. Was, CERN-TH-6230-91 (Sept. 1991); S. Jadach, E. Richter-Was, B.F.L. Ward, and Z. Was, Phys. Lett. B268 (1991) 253; S. Jadach and B.F.L. Ward, Phys. Rev. D 40 (1989) 3582; S. Jadach, E. Richter-Was, B.F.L. Ward, and Z. Was, Phys. Lett. B260 (1991) 438; S. Jadach, E. Richter-Was, B.F.L. Ward, and Z. Was, Phys. Lett. B253 (1991) 469. Version 1.22 was obtained from B. Ward for this application.
12. F. Berends and R. Kleiss, Nucl. Phys. B186 (1981) 22.
13. F. Berends, R. Kleiss, and S. Jadach, Nucl. Phys. B202 (1982) 63.
14. R. Kleiss and S. van der Marck, Nucl. Phys. B342 (1990) 61.
15. All the data shown in plots represents a uniform sampling of events from the $\sim$2.5 fb^{-1} dataset. Bhabhas, photon pairs, and muon pairs were prescaled at rates of 1/50, 1/5, and 1/2, respectively, to yield $\sim$0.5M events for each process.
16. S. Jadach and Z. Was, Comp. Phys. Comm. 36 (1985) 191; S. Jadach and Z. Was, Comp. Phys. Comm. 64 (1991) 267; S. Jadach, J.H. Kuhn, and Z. Was, Comp. Phys. Comm. 64 (1991) 275; M. Jezabek, Z. Was, S. Jadach, and J.H. Kuhn, CERN-TH-6195-91 (Aug. 1991).
17. V.M. Budnev, *et al.*, Phys. Rep. C15 (1975) 181.
18. J. Vermasseren, Nucl. Phys. B229 (1983) 347.
19. For this article, the small proportion of CLEO II data taken at the $\Upsilon(1S)$ and $\Upsilon(3S)$ resonances was excluded to eliminate complications of direct resonance decays to dileptons. Of the remaining data, two-thirds were taken near the peak of the $\Upsilon(4S)$ at E_b=5.29 GeV and the balance on the "continuum" near 5.26 GeV.

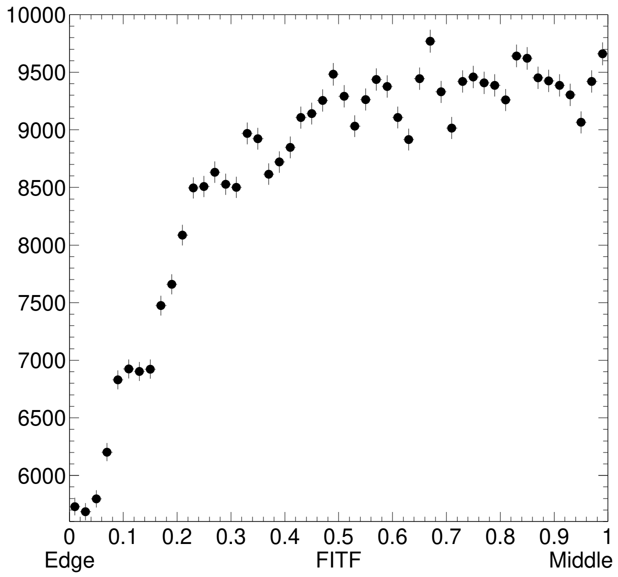

Fig. 1. Distribution on $\mu-$pair events of ϕ_{TF}, the projected μ^+ azimuthal intercept, modulo a half-TF counter width. ϕ_{TF}=0 corresponds to a counter edge and ϕ_{TF}=1 is the counter center. The falloff for ϕ_{TF}<0.5 is due to trigger inefficiency near TF counter edges and crystal-grouping boundaries.

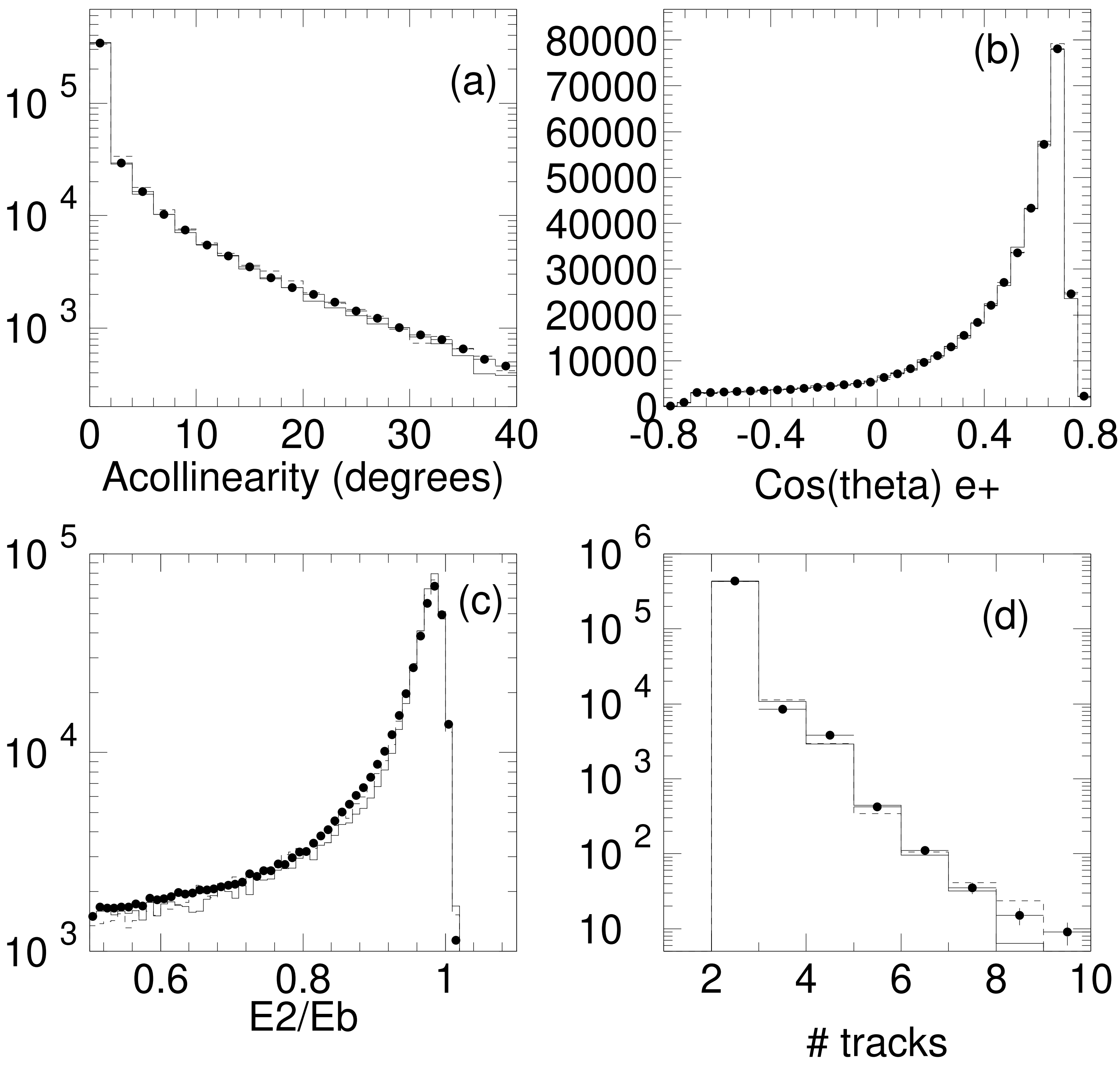

Fig. 2. Distributions on Bhabha events for data (solid circles), BHLUMI Monte Carlo (solid histogram), and BKee Monte Carlo (dashed histogram) in (a) acollinearity of the two tracks; (b) cosθ of the positron; (c) the smaller of the top two shower energies, scaled to the beam energy; and (d) charged track multiplicity.

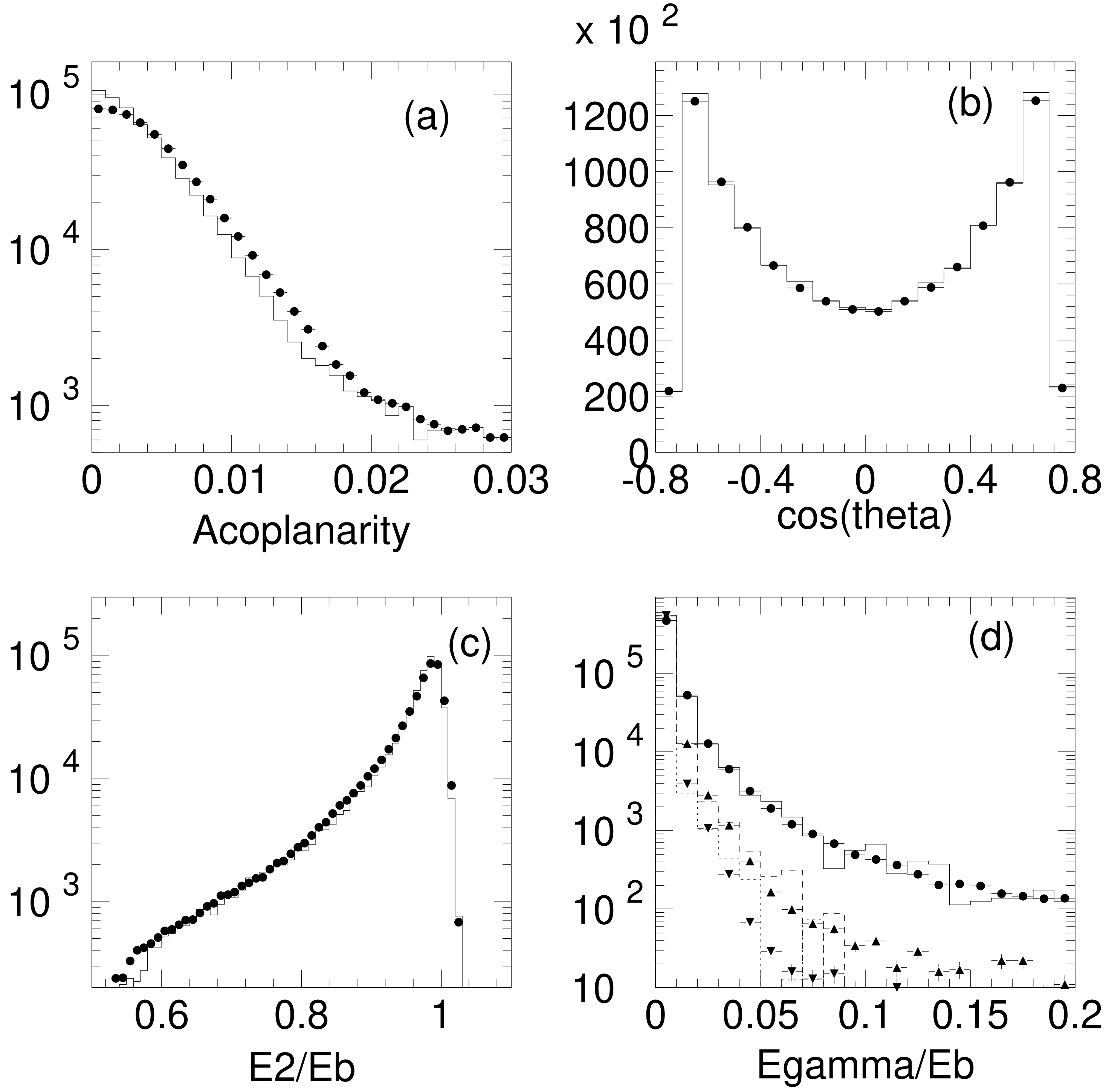

Fig. 3. Distributions on $\gamma\gamma$ events for data (solid circles) and BK$\gamma\gamma$ Monte Carlo (solid histogram) in (a) shower acoplanarity; (b) $\cos\theta$ of the two highest energy photon showers (two entries/event); (c) the energy of the second highest energy photon, scaled to the beam energy; and (d) the energy of the third, fourth, and fifth highest energy photon, scaled to the beam energy, shown in solid circles, upward- and downward-pointing triangles for the data and solid, dashed, and dotted histograms for the Monte Carlo, respectively.

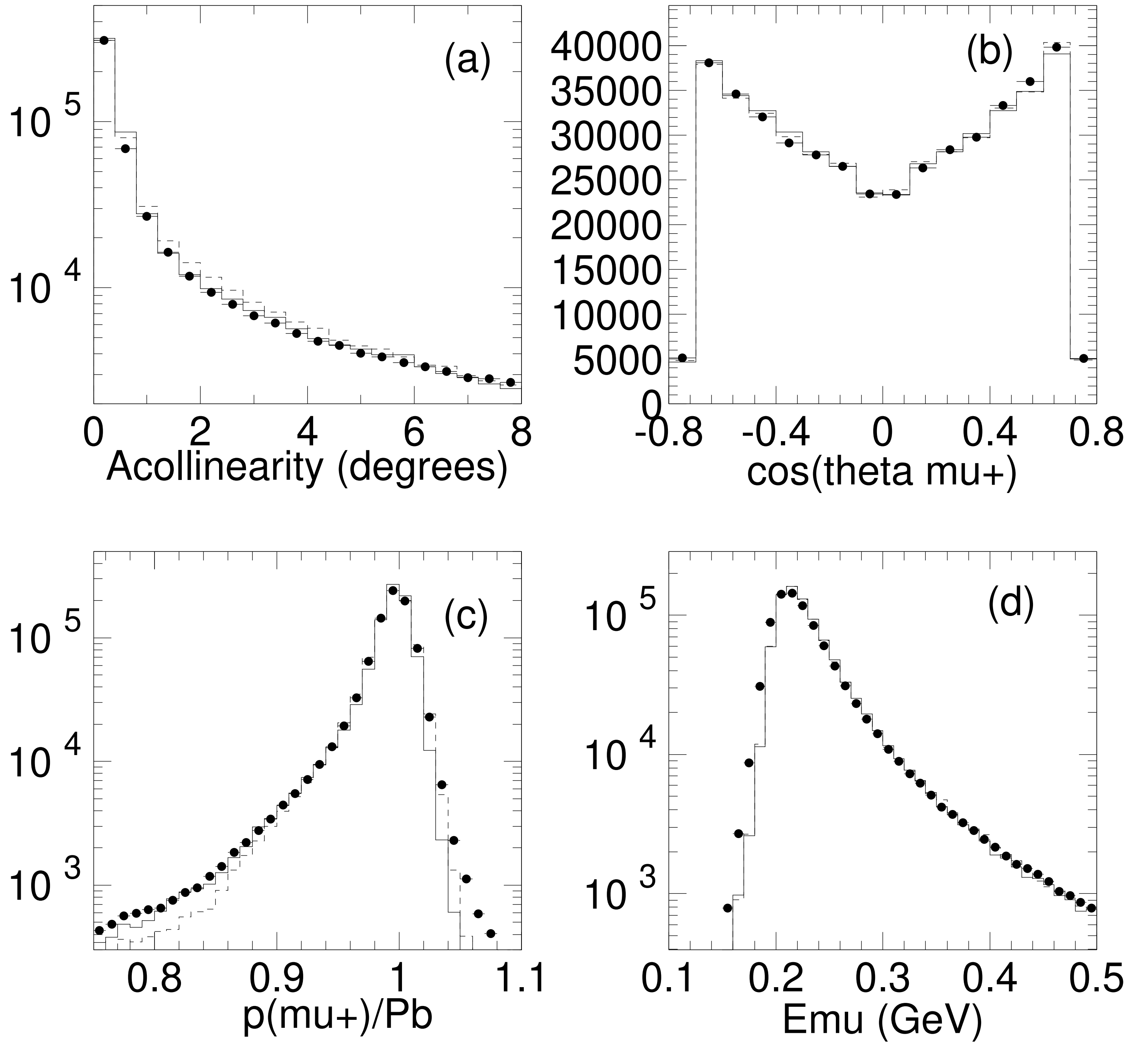

Fig. 4. Distributions on $\mu-$pair events for data (solid circles), FPAIR Monte Carlo (solid histogram), and BKJ Monte Carlo (dashed histogram) in (a) acollinearity of the two tracks; (b) $\cos\theta$ of the μ^+; (c) momentum of each track scaled to the beam momentum (two entries/event); and (d) energy deposited in the calorimeter by each muon (two entries/event).

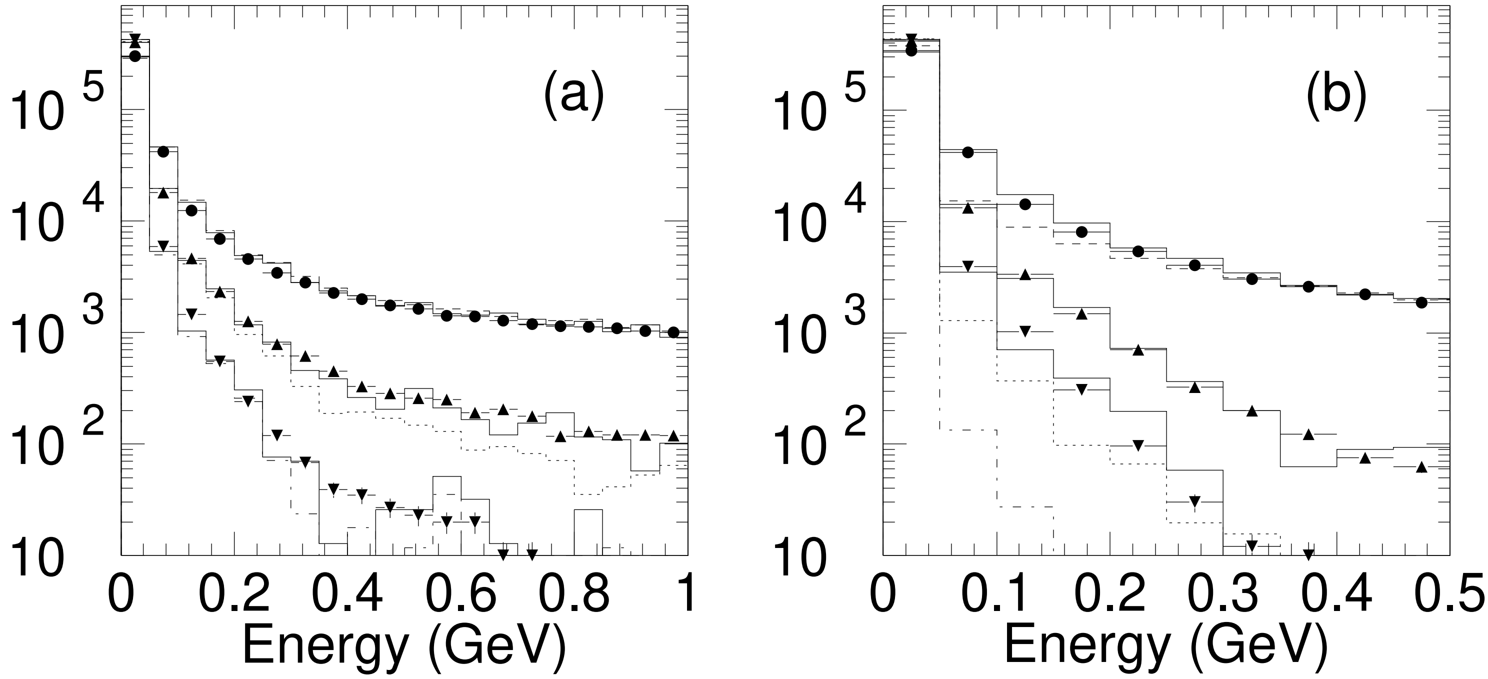

Fig. 5. Distributions in the energy of the first, second, and third most energetic photon per event for data (solid circles, upward- and downward-pointing triangles), α^4 Monte Carlo (solid histograms), and α^3 Monte Carlo (dashed, dotted, and dot-dashed histograms), respectively, for (a) e^+e^- events, and (b) $\mu^+\mu^-$ events.

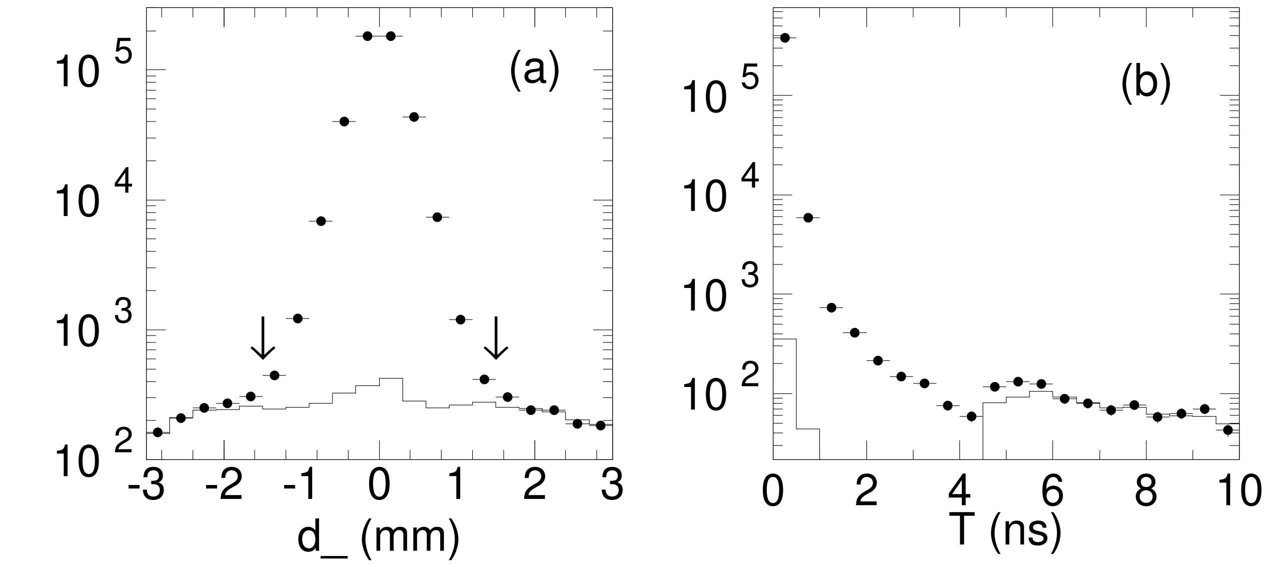

Fig. 6. Distribution on $\mu-$pair and cosmic ray events of (a) impact parameter for the negative track d_-, and (b) time-of-flight variable T. In (a), the data are shown with the $d_\pm$ cut relaxed (solid circles); cosmic rays are selected with $T > 4$ ns (histogram) and normalized for $|d_-| >2$ mm. The arrows indicate the default requirement $|d_\pm| <1.5$ mm. In (b), cosmic rays (histogram) are selected with $|d_-| >2$ mm and normalized for $T >6$ ns.

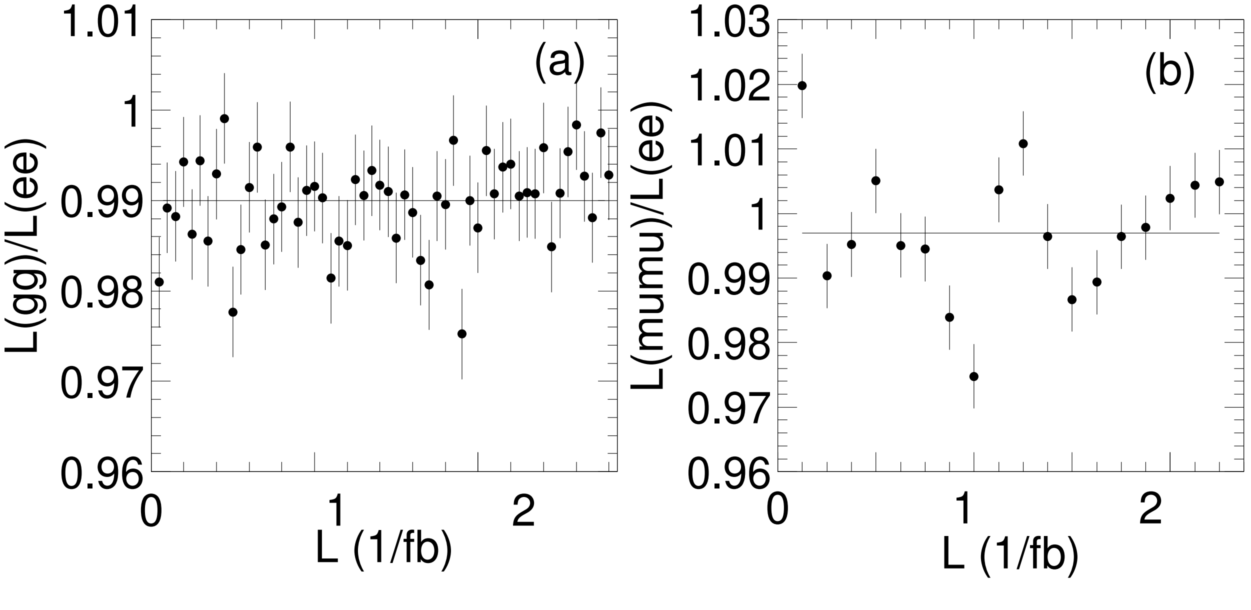

Fig. 7. Ratio of different measures of luminosity as a function of integrated luminosity: (a) $\mathcal{L}(\gamma\gamma)/\mathcal{L}(e^+e^-)$ in bins of $\sim$40 pb^{-1}; and (b) $\mathcal{L}(\mu^+\mu^-)/\mathcal{L}(e^+e^-)$ in bins of $\sim$125 pb^{-1}.